Coordinated Planning of Interconnected Multi-regional Power Systems Considering Large-scale Energy Storage Systems, Transmission Expansion, and Carbon Emission Quota Trading

Jia Liu, *Member*, *IEEE*, *Member*, *CSEE*, Biao Jiang, Zao Tang, *Member*, *IEEE*, Pingliang Zeng, *Senior Member*, *IEEE*, *Senior Member*, *CSEE*, Tong Su, Yalou Li, *Senior Member*, *IEEE*, *Senior Member*, *CSEE*, and Qiuwei Wu, *Senior Member*, *IEEE*

***Abstract*—Global warming has motivated the world's major countries to actively develop technologies and make policies to promote carbon emission reduction. Focusing on interconnected multi-regional power systems, this paper proposes a coordinated planning model for interconnected power systems considering energy storage system planning and transmission expansion. A market-based carbon emission quota trading market that helps reduce carbon emissions is built and integrated into the coordinated planning model, where entities can purchase extra or sell surplus carbon emission quotas. Its effects on promoting carbon emission reduction are analyzed. Considering the limitations on information exchange between interconnected regional power systems, the proposed model is decoupled and solved with the analytical target cascading algorithm. A modified two-region 48-bus system is used to verify the effectiveness of the proposed model and solving method.**

***Index Terms*—Analytical target cascading algorithm, energy storage system, multi-regional power system, tiered pricing mechanism, transmission expansion planning.**

NOMENCLATURE

A. Parameters

D_s	Number of time intervals of the year in scenario s.
r_0	Annual interest rate.
m	Equipment lifetime.
$c_{ij,l}$	Investment cost of the l-th line between bus i and j (M$).
c_{en}	Investment cost per MWh for ESS ($/MWh).
c_{pow}	Investment cost per MW for ESS ($/MW).
c_{co_2}	Carbon emission trading base price ($/t$CO_2$).
$\tilde{c}_l$	Maximum line investment budget ($).
$\tilde{c}_b$	Maximum ESS investment budget ($).
a_g, b_g, c_g	Cost coefficients of thermal power unit g.
c^{wc}	Penalty cost for wind curtailment ($/MWh).
$P^{\max}_{s,w,t}$	Maximum output of wind power w at time t in scenario s (MW).
$b_{ij,l}$	Susceptance of the l-th line between bus i and bus j.
L_1	Length of the carbon emission trading price interval.
$F^{\min}_{ij,l}, F^{\max}_{ij,l}$	Minimum and maximum capacities of the l-th line between bus i and bus j, respectively (MW).
$P^{\min}_g, P^{\max}_g$	Minimum and maximum power outputs of the thermal power unit g (MW).
$P^{\max}_{ij}$	Maximum power on the tie-line at the connecting bus i, j of the two regions in scenario s (MW).
RU_g, RD_g	Ramp-down and ramp-up limits of the thermal power unit g (MW/h).
RU_l, RD_l	Ramp-down and ramp-up limits of tie-line l (MW/h).
$T^{\mathrm{on}}_g, T^{\mathrm{off}}_g$	Minimum startup and shut down times of the thermal power unit g (h).
$E^{\min}_b, E^{\max}_b$	Minimum and maximum capacities of the installed ESS b (MWh).
$P^{\min}_b, P^{\max}_b$	Minimum and maximum power of the installed ESS b (MW).
σ_b	Self-discharge efficiency of ESS b.
η	Carbon emission quota factor (tCO_2/MWh).
$\eta_{b,c}, \eta_{b,d}$	Charge and discharge coefficients of the ESS b.
μ	Energy-to-power time for ESS (h).
δ_g	Carbon emission factor of unit g (tCO_2/MWh).
τ_1	Growth coefficient of the carbon trading price.
Δt	Time Duration of a time interval (h).

Manuscript received July 26, 2023; revised September 15, 2023; accepted December 17, 2023. Date of online publication January 10, 2025; date of current version March 3, 2025. This work was supported by the National Nature Science Foundation of China under Grants U2166211 and 52207085.

J. Liu and Z. Tang (corresponding author, email: ztang@hdu.edu.cn) are with the Department of Automation, Hangzhou Dianzi University, Hangzhou 310018, China, and also with the Department of Electrical Engineering, Southeast University, Nanjing 210096, China.

B. Jiang and P. L. Zeng are with the Department of Automation, Hangzhou Dianzi University, Hangzhou 310018, China.

T. Su is with the University of Connecticut, Storrs 06279, USA.

Y. L. Li is with China Electric Power Research Institute, Beijing 100192, China.

Q. W. Wu is with the Department of Electrical Engineering, Technical University of Denmark, Kongens Lyngby 2800, Denmark.

DOI: 10.17775/CSEEJPES.2023.06230

B. Variables

C_{line}	Line investment cost.
C_{Ess}	ESS investment cost.
C_{Gen}	Generation cost.
C_W	Wind curtailment cost.
$C_{c,s,g,t}$	Carbon emission trading cost of the unit g at time t in scenario s.
C_c	Carbon emission trading cost.
$E^e_{s,g,t}$	Carbon emission quota of the unit g at time t in scenario s.
$E^q_{s,g,t}$	Carbon emission of the unit g at time t in scenario s.
$E_{s,g,t}$	Traded carbon emission quota of unit g at time t in scenario s.
$I_{ij,l}$	Binary variable indicating whether the l-th candidate is constructed or not between bus i and bus j.
$f_{s,ij,l,t}$	Power flow on the l-th line between starting bus i and bus j at time t in scenario s.
$P_{s,g,t}$	Output power of unit g at time t in scenario s.
$P_{s,w,t}$	Output of wind farm w at time t in scenario s.
$P^c_{s,b,t}, P^d_{s,b,t}$	Charging and discharging power of ESS b at time t in scenario s.
S_b, P_b	Capacity and Power of installed ESS b (MWh/MW).
$S_{s,b,t}$	Stored energy of ESS b at time t in scenario s (MWh).
$u_{s,g,t}$	On/Off state of the thermal power unit g at time t in scenario s.
$u^c_{s,b,t}, u^d_{s,b,t}$	Charging and discharging modes of ESS b at time t in scenario s.
x_b	Binary variable indicating whether the b-th ESS is constructed or not.
$\theta_{s,i,t}$	Phase angle between bus i at time t in scenario s (rad).

C. Sets

B	Set of candidate ESS.
B_i	Set of ESS at bus *i.*
G	Set of thermal power units.
G_i	Set of the thermal power units at bus i.
K, K^+, K^-	Sets of all, candidate and existing transmission lines.
W	Set of wind power.
W_i	Set of wind power at bus *i.*
T	Set of time intervals.
S	Set of scenarios.
Ω	Set of buses.
$\Omega_{\text{rec}(i)}$	Set of lines with bus i as the receiving bus.
$\Omega_{\text{sen}(i)}$	Set of lines with bus i as the sending bus.

I. INTRODUCTION

IN recent years, global warming has received increasing international attention. The world's major countries have been actively developing technologies and making policies to promote carbon emission reduction. In this context, promoting the development and accommodation of zero-emission renewable energy, such as wind and solar energy, has become one of the most effective measures to pave the way to carbon emission reduction. However, renewable energy curtailment is almost inevitable due to the uncertainty of renewable energy. Energy storage systems (ESS) [1], [2] and multi-regional interconnection [3], [4] are essential reliance for improving renewable energy accommodation and eventually realizing carbon emission reduction.

From a system operation perspective, commonly used methods for reducing carbon emissions include enforcing carbon emission limitations [5], [6], implementing carbon emission quota trading [7], [8], and adopting low-carbon power generation technology [9]–[11]. In reference [6], two carbon emission cost models are discussed, and the influence of carbon emission quota trading on transmission expansion planning is discussed. Reference [12] proposed a low-carbon planning model that, on the one hand, incorporates the cost of low-carbon generation technology and the carbon emission quota cost into the objective and on the other hand, includes the carbon emission reduction target as a constraint. Reference [13] proposed a carbon flow tracking method to allocate carbon emissions to electricity consumers and assign the responsibility for carbon emissions to the load side. Based on carbon emission flow theory, reference [14] proposed a low-carbon optimal scheduling model particularly for systems equipped with carbon capture systems. In reference [15] and [16], the carbon emission quota price in transmission expansion planning is modeled with a probability density function, and the Monte Carlo method was used to generate prices reflecting their fluctuations. Reference [17] proposed a low-carbon economy-oriented power generation expansion planning model, which comprehensively considers the influence of factors such as carbon capture power plant retrofit and carbon emission costs on the planning process. Reference [18] studied the impact of carbon emission quota trading and wind energy integration on carbon emission in the power dispatching process to obtain an optimal dispatching scheme according to the real-time carbon emission quota price.

The above models focus merely on reducing carbon emissions while ignoring the most prominent characteristic of emerging power systems – high penetration of renewable energy. Enhancing the integration of renewable energy sources is also a method to reduce carbon emissions. Reference [19] proposed a low-carbon economic dispatch model considering carbon capture systems, wind energy, and ESSs. The result verifies the model's effectiveness in helping reduce both carbon emission and wind power curtailment. References [20] and [21] studied wind-storage hybrid systems. In those systems, ESSs are integrated to help reduce the fluctuations of wind energy. References [22]–[24] proposed a coordinated planning model of transmission expansion and ESS, especially focusing on systems with high wind energy penetration. For large-scale ESSs, reference [25] proposed a stochastic programming base model to determine the reserve against wind energy fluctuations. The above works demonstrate the importance of utilizing ESSs to effectively accommodate renewable energy, such as wind energy while reducing carbon emissions.

The aforementioned models are all centralized models, and

they need to access the data of the entire power system during the calculation process. However, with the continuous development of power systems, large power systems usually consist of multiple sub-regions, which makes distributed algorithms more suitable. Distributed algorithms are increasingly widely used to solve the planning problems of interconnected power systems due to their scalability, privacy protection and limited information exchange. Alternating Direction Method of Multipliers (ADMM) algorithm [26]–[28], Auxiliary Problem Principle (APP) algorithms [29], [30], and Analytical Target Cascading (ATC) algorithms [31]–[33] are the most popular distributed algorithms being widely used. Reference [34] proposed a fully distributed optimization algorithm to realize the coordinated transmission expansion planning crossing multi-regional power systems. Reference [35] used the ADMM algorithm to solve a low-carbon economic scheduling model of a distributed power system equipped with carbon capture systems. It integrated a carbon emission quota trading mechanism. To ensure the optimal operation of transmission and distribution networks, some works, such as references [36] and [37], built transmission and distribution coordinated models and solved them using distributed algorithms. Additionally, reference [38] proposed an ATC-based transmission network structure optimization model for transmission expansion planning to fully use renewable energy and enhance the interconnection and coordination of multi-regional power systems. These works demonstrate the applicability and effectiveness of distributed algorithms in power system planning.

ESS and coordination of multi-regional systems are important for realizing renewable energy accommodation and carbon emission reduction. It is worthwhile to emphasize that the buildable capacities of ESSs are limited by factors such as technology and geographical locations. This paper proposes a coordinated planning model focusing on interconnected multi-regional power systems considering ESS planning, transmission expansion, and carbon emission quota trading under the high wind energy penetration. The main contributions of this paper are as follows:

1) A coordinated planning model focusing on interconnected multi-regional power systems considering ESS planning and transmission expansion is proposed.

2) The coordinated planning model integrates Carbon emission quota trading. Its effects on promoting carbon emission reduction are analyzed.

3) To address the privacy concerns of information exchange between individual power systems within a multi-regional power system, a distributed algorithm is utilized to solve the model.

The rest of the structure is as follows: Section II presents the tiered-pricing base carbon emission trading mechanism; Section III proposes the multi-regional power system planning model; Section IV discusses the solution methodology; Section V presents the case study; and Section VI concludes this paper.

II. Tiered-pricing Base Carbon Emission Trading Mechanism

As shown in Fig. 1, the market-based carbon emission quota trading mechanism helps reduce greenhouse gas emissions by building a market where companies can purchase extra or sell surplus carbon emission quotas, i.e., allocated carbon gas emission credits. Economic incentives motivate companies to reduce their greenhouse gas emissions effectively, paving the way for achieving the carbon emission reduction target.

Practical implementation of the carbon emission quota trading market requires unified carbon emission reduction targets, solid carbon emission limits, and effective emission quota allocation methods, which further necessitates cooperation and coordination between governments and international organizations to create a stable and fair carbon emission quota market environment.

The price signals generated from the carbon emission quota trading market that reflect the supply and demand relationship of carbon emission quotas should incentivize quota demanders to transform their production and development more environmentally friendly, thereby eventually promoting carbon emission reduction. Although debates still exist about the allocation method of carbon emission quotas in both academic and industry fields regarding different perspectives, such as fairness and efficiency, two main categories of methods, i.e., paid allocation-based methods and free allocation-based methods, have come to the fore. Currently carbon emission quota

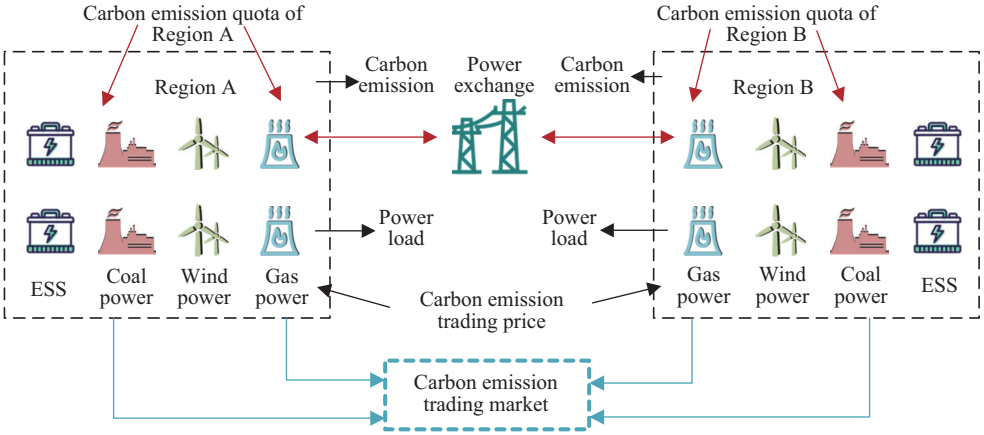

Fig. 1. Carbon emission quota trading market.

trading markets in China are in the early stages. The power industry adopts the baseline method – a free allocation-based method, to primarily motivate market activity and ultimately carbon emission reduction [39]. The baseline method can calculate the free carbon emission quota as in (1). Thermal units are the power system's main source of carbon emissions, and their carbon emissions can be calculated by (2). Based on (1) and (2), the carbon emission quota trading model of thermal units can be formulated as in (3).

$$E^{e}_{s,g,t} = \eta P_{s,g,t} \Delta t \tag{1}$$

$$E^{q}_{s,g,t} = \delta_g P_{s,g,t} \Delta t \tag{2}$$

$$E_{s,g,t} = E^{q}_{s,g,t} - E^{e}_{s,g,t} \tag{3}$$

In (3), a negative $E^{q}_{s,g,t} - E^{e}_{s,g,t}$ means that the carbon emission of unit g exceeds its quota, which requires purchasing extra carbon emission quotas and increases operating costs. On the contrary, a positive $E^{q}_{s,g,t} - E^{e}_{s,g,t}$ means the carbon emission quota of unit g still has a surplus after deducting its usage. The surplus can be sold for profit, bringing operating costs offset.

A tiered pricing mechanism is proposed in this paper to effectively reduce the carbon emissions of power generation companies. The carbon emission quota is offered with multiple tiers composed of different amounts and prices as shown in Fig. 2. For a tier, the price corresponds to a certain amount of carbon emission quotas. Therefore, for example, if a company desires a larger carbon emission quota, the total cost rises proportionally with the amount and increases with the increasing unit price. This tiered pricing mechanism could generate economic incentives to motivate companies to reduce their carbon emissions and produce in a more environmentally friendly way. A company should optimally purchase an appropriate carbon emission quota and, based on that, manage its carbon emissions, achieving sustainable development and environmental protection.

Based on the tiered prices for different amounts, the carbon emission quota trading costs of generator g at scenario s and time t can be calculated as in (4).

$$C_{c,s,g,t} = \begin{cases} c_{co_2} E_{s,g,t}, E_{s,g,t} \le L_1 \\ c_{co_2} L_1 + c_{co_2}(1+\tau_1)(E_{s,g,t} - L_1), L_1 < E_{s,g,t} \le 2L_1 \\ c_{co_2} L_1(2+\tau_1) + c_{co_2}(1+2\tau_1)(E_{s,g,t} - 2L_1), \\ \quad 2L_1 < E_{s,g,t} \le 3L_1 \\ c_{co_2} L_1(3+3\tau_1) + c_{co_2}(1+3\tau_1)(E_{s,g,t} - 3L_1), \\ \quad 3L_1 < E_{s,g,t} \le 4L_1 \\ c_{co_2} L_1(4+6\tau_1) + c_{co_2}(1+4\tau_1)(E_{s,g,t} - 4L_1), \\ \quad E_{s,g,t} > 4L_1 \end{cases} \tag{4}$$

III. Multi-regional Power System Planning

The planning problem of a regional system is typically conducted by the regional power grid company that administrates the grid, such as a provincial power grid company. In planning a regional system, new tie lines interconnecting two regions are not considered.

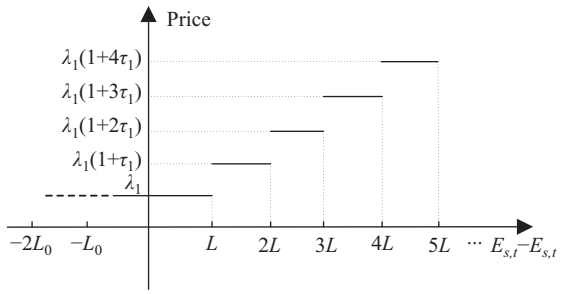

Fig. 2. The tiered pricing of carbon emission quota.

In this paper, the coordination of multiple regional power systems that are interconnected with tie lines is considered. An example is shown in Fig. 3. The variable representing power flow on the tie line is duplicated for Region A and Region B as $P^{A}_{s,i,t}$ and $P^{B}_{s,j,t}$. They are enforced to be equal as in (5) considering the preset positive direction of power flowing from Region A to Region B. With this setting, for Region B, Region A can be treated as a virtual power plant, while for Region A, Region B can be considered as a virtual load. If the power flowing from Region A to Region B is negative, namely $P^{A}_{s,i,t} < 0$, the actual flow is from Region B to Region A.

$$P^{A}_{s,i,t} = P^{B}_{s,j,t} \tag{5}$$

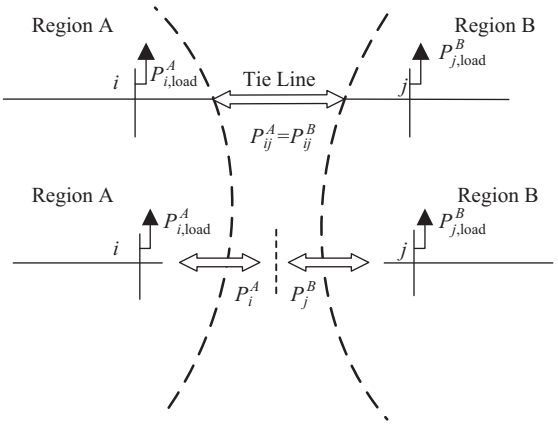

Fig. 3. Multi-regional power system decoupling.

A. Objective function

As in (6), the objective of the proposed multi-regional power system planning model is to minimize the total cost of the power system. The objective comprises five terms: the investment cost of transmission lines, the investment cost of ESSs, the generation cost, the wind curtailment penalty, and the cost of carbon emission quotas. The five terms are respectively detailed in (7).

$$\min C = C_{\text{line}} + C_{\text{Ess}} + C_{\text{Gen}} + C_W + C_c \tag{6}$$

$$C_{\text{line}} = \frac{r_0(1+r_0)^m}{(1+r_0)^m - 1} \sum_{l \in K^+} c_{ij,l} I_{ij,l}$$

$$C_{\text{Ess}} = \frac{r_0(1+r_0)^m}{(1+r_0)^m - 1} \sum_{b \in B} x_b (c_{\text{en}} S_b + c_{\text{pow}} P_b)$$

$$C_{\mathrm{Gen}}=\sum_{s\in S}D_s\sum_{t\in T}\sum_{g\in G}(a_g+b_gP_{s,g,t}+c_gP_{s,g,t}^2)$$
$$C_W=\sum_{s\in S}D_s\sum_{t\in T}\sum_{w\in W}c^{wc}(P_{s,w,t}^{\max}-P_{s,w,t})$$

$$C_c=\sum_{s\in S}D_s\sum_{t\in T}\sum_{g\in G}C_{c,s,g,t} \tag{7}$$

In the first term of (7), $I_{ij,l}=1$ indicates the construction of transmission lines. Otherwise it is 0. The second term represents the investment cost of ESS, which is related to the installed capacity and energy. The third term represents the generation cost calculated with quadratic cost curves. Notably, a piecewise linearization approach is employed in the calculation based on reference [40]. The fourth term represents curtailed energy costs, and the fifth represents the carbon emission quota trading cost.

B. Constraints

The constraints of the proposed multi-regional power system planning model are detailed in the following.

1) Investment Constraint

$$\sum_{l\in K^+}c_{ij,l}I_{ij,l}\le\tilde{c}_l,\ \forall(i,j)\in\Omega,\ \forall l\in K^+ \tag{8}$$
$$\sum_{b\in B}x_b(c_{\mathrm{en}}S_b+c_{\mathrm{pow}}P_b)\le\tilde{c}_b,\ \forall b\in B \tag{9}$$

Constraints (8) and (9) effectively limit the total investments on transmission lines and ESSs.

2) Flow Limits of Existing Lines

$$f_{s,ij,l,t}=b_{ij,l}(\theta_{s,i,t}-\theta_{s,j,t})$$
$$\forall(i,j)\in\Omega,\ \forall l\in K^-,\ \forall t\in T,\ \forall s\in S \tag{10}$$
$$F_{ij,l}^{\min}\le f_{s,ij,l,t}\le F_{ij,l}^{\max}$$
$$\forall(i,j)\in\Omega,\ \forall l\in K^-,\ \forall t\in T,\ \forall s\in S \tag{11}$$

Constraint (10) calculates the power flows on the existing transmission lines. Power flows on existing transmission lines are limited by constraint (11).

3) Flow Limits of the Candidate Lines

$$\begin{cases}(1-I_{ij,l})M\le f_{s,ij,l,t}-b_{ij,l}(\theta_{s,i,t}-\theta_{s,j,t})\\ f_{s,ij,l,t}-b_{ij,l}(\theta_{s,i,t}-\theta_{s,j,t})\le(1-I_{ij,l})M\\ \forall(i,j)\in\Omega,\ \forall l\in K^+,\ \forall t\in T,\ \forall s\in S\end{cases} \tag{12}$$
$$I_{ij,l}F_{ij,l}^{\min}\le f_{s,ij,l,t}\le I_{ij,l}F_{ij,l}^{\max}$$
$$\forall(i,j)\in\Omega,\ \forall l\in K^+,\ \forall t\in T,\ \forall s\in \tag{13}$$

Once candidate line l is planned, namely $I_{ij,l}=1$, constraint (12) corresponding to line l is enforced and the flow it carries is calculated as $f_{s,ij,l,t}=b_{ij,l}(\theta_{s,i,t}-\theta_{s,j,t})$; otherwise, $I_{ij,l}=0$, constraint (9), i.e., $f_{s,ij,l,t}$, is relaxed. The power flow on candidate line l is further limited by constraint (13).

4) Thermal Power Unit Operational Constraints

$$u_{s,g,t}P_g^{\min}\le P_{s,g,t}\le u_{s,g,t}P_g^{\max}$$
$$\forall t\in T,\ \forall g\in G,\ \forall s\in S \tag{14}$$
$$u_{s,g,t}-u_{s,g,t-1}-u_{s,g,\tau}\le 0,\ \tau\in[t,\min(T,t+T_g^{\mathrm{on}}-1)]$$
$$\forall t\in T,\ \forall g\in G,\ \forall s\in S \tag{15}$$
$$u_{s,g,t-1}-u_{s,g,t}-u_{s,g,\tau}\le 1,\tau\in[t,\min(T,t+T_g^{\mathrm{off}}-1)]$$
$$\forall t\in T,\ \forall g\in G,\ \forall s\in S \tag{16}$$
$$P_{s,g,t}-P_{s,g,t-1}+u_{s,g,t-1}(P_g^{\min}-RU_g)$$
$$+u_{s,g,t}(P_g^{\max}-P_g^{\min})\le P_g^{\max}$$
$$\forall t\in T,\ \forall g\in G,\ \forall s\in S \tag{17}$$
$$P_{s,g,t-1}-P_{s,g,t}+u_{s,g,t}(P_g^{\min}-RD_g)$$
$$+u_{s,g,t-1}(P_g^{\max}-P_g^{\min})\le P_g^{\max}$$
$$\forall t\in T,\ \forall g\in G,\ \forall s\in S \tag{18}$$

Constraint (14) represents the generation output constraint for thermal units. Constraints (15) and (16) enforce thermal units' minimum ON/OFF time. Constraints (17) and (18) limit their ramp-up and ramp-down rates considering unit startup and shutdown.

5) Wind Farm Constraints

$$0\le P_{s,w,t}\le P_{s,w,t}^{\max},\ \forall t\in T,\ \forall w\in W,\ \forall s\in S \tag{19}$$

Constraint (19) ensures that the scheduled wind power is within the forecast at any given time interval.

6) ESS Investment Constraints

$$x_bE_b^{\min}\le S_b\le x_bE_b^{\max},\ \forall b\in B \tag{20}$$
$$x_bP_b^{\min}\le P_b\le x_bP_b^{\max},\ \forall b\in B \tag{21}$$
$$P_b\mu\le S_b,\ \forall b\in B \tag{22}$$

The maximum power and installed capacity of candidate ESSs are respectively bounded by (20) and (21). In addition, the maximum power of a candidate ESS should be related to its capacity as in (22).

7) ESS Operation Constraints

$$0\le P_{s,b,t}^d\le u_{s,b,t}^dP_b,\ \forall t\in T,\ \forall b\in B,\ \forall s\in S \tag{23}$$
$$0\le P_{s,b,t}^c\le u_{s,b,t}^cP_b,\ \forall t\in T,\ \forall b\in B,\ \forall s\in S \tag{24}$$
$$0\le S_{s,b,t}\le S_b,\ \forall t\in T,\ \forall b\in B,\ \forall s\in S \tag{25}$$
$$S_{s,b,t}=S_{s,b,t-1}(1-\sigma_b)+P_{s,b,t}^c\eta_{b,c}\Delta t-\frac{P_{s,b,t}^d\Delta t}{\eta_{b,d}}$$
$$\forall t\in T,\ \forall b\in B,\ \forall s\in S \tag{26}$$
$$S_{s,b,1}=S_{s,b,T},\ \forall b\in B,\ \forall s\in S \tag{27}$$
$$u_{s,b,t}^c+u_{s,b,t}^d\le 1,\ \forall t\in T,\ \forall b\in B,\ \forall s\in S \tag{28}$$
$$u_{s,b,t}^c,u_{s,b,t}^d\in\{0,1\},\ \forall t\in T,\ \forall b\in B,\ \forall s\in S \tag{29}$$

Constraints (23)–(24) limit the maximum charging and discharging power of an ESS. Constraint (25) limits the stored energy to be within the capacity. Constraint (26) calculates the stored energy of the ESS at time t. Constraint (27) enforces that the stored energy of the ESS at the initial time interval is equal to that at the terminal time interval. Constraint (28), where $u_{s,b,t}^c$ and $u_{s,b,t}^d$ are binaries, forbids simultaneously charging and discharging.

8) Nodal Power Balance Constraints

$$\sum_{g\in G_i} P_{s,g,t} + \sum_{w\in W_i} P_{s,w,t} + \sum_{j\in\Omega_{\mathrm{rec}(i)}}\sum_{l\in K} f_{s,ij,l,t} - \sum_{j\in\Omega_{\mathrm{sen}(i)}}\sum_{l\in K} f_{s,ij,l,t} + \sum_{b\in B_i} P^d_{s,b,t} - \sum_{b\in B_i} P^c_{s,b,t} = P^l_{s,i,t} \tag{30}$$

Constraint (30) enforces the nodal power balance.

9) Tie-line Constraints Among Multiple Regions

$$P_{s,ij,t} = b_{ij,l}(\theta_{s,i,t} - \theta_{s,j,t}) \quad \forall (i,j)\in\Omega,\ \forall t\in T,\ \forall s\in S \tag{31}$$

$$-P^{\max}_{ij} \le P_{s,ij,t} \le P^{\max}_{ij} \quad \forall (i,j)\in\Omega,\ \forall t\in T,\ \forall s\in S \tag{32}$$

$$RD_l\Delta t \le P_{s,ij,t} - P_{s,ij,t-1} \le RU_l\Delta t \quad \forall (i,j)\in\Omega,\ \forall t\in T,\ \forall s\in S \tag{33}$$

Constraints (31) calculates the power flow on tie lines interconnecting two regions. On the one hand, $P_{s,ij,t}$ are limited by the line flow limits and on the other hand, their variations over two consecutive time intervals are limited to mitigate the variations of tie-lines. Ramp-up and ramp down constraints for tie-line power are formulated in (33).

IV. Solving Methodology

This paper presents a distributed expansion planning iteration divided into two parts: the bi-level planning problem within each region and the optimization problem of inter-regional power transmission consistency. The Column-and-Constraint Generation (C&CG) algorithm is used to solve the first problem, while the ATC algorithm is utilized to solve the second problem.

A. Solving the Planning Model of Individual Regions

The planning model of each region forms a bi-level programming problem that involves investment and operation decisions. The paper employs the C&CG algorithm to solve the planning model of individual regions. The planning model of a region can be reformulated as in the following:

$$\min_x \boldsymbol{c}^{\mathrm{T}}\boldsymbol{x} + \boldsymbol{b}^{\mathrm{T}}\boldsymbol{y} \tag{34}$$

$$\text{s.t.}\quad \boldsymbol{A}\boldsymbol{x} \le \boldsymbol{e}, \boldsymbol{x}\in\{0,1\} \tag{35}$$

$$\min_y \boldsymbol{b}^{\mathrm{T}}\boldsymbol{y} \tag{36}$$

$$\text{s.t.}\quad \boldsymbol{F}\boldsymbol{y} = \boldsymbol{g},\ \boldsymbol{G}\boldsymbol{y} \le \boldsymbol{k},\ \boldsymbol{H}\boldsymbol{y} \le \boldsymbol{m} - \boldsymbol{J}\boldsymbol{x} \tag{37}$$

We use $\boldsymbol{x}$ to represent the investment decisions made in the upper level and $\boldsymbol{y}$ to represent operational decisions in the inner level. $\boldsymbol{c}^{\mathrm{T}}\boldsymbol{x}$ represents the investment cost and $\boldsymbol{b}^{\mathrm{T}}\boldsymbol{y}$ represents the operating cost, which is composed of the generation cost, wind curtailment cost, and the cost for carbon emission quotas. Constraint (35) in a compact form includes constraints (8)–(9), (15)–(16), and (28), while constraint (37) represents constraints (10)–(14), (17)–(27), (30)–(33).

The process of solving the bi-level programming problem (34)–(37) is as follows:

Step 1: Initialize the lower bound LB as $-\infty$, the upper bound UB as $-\infty$, the iteration number n as 1, and the convergence tolerance φ as 10^{-6}.

Step 2: Let $n = n + 1$ and then solve the master problem (34)–(35) to obtain the optimal solution $\boldsymbol{x}^*_n$ to investment decisions and update the lower bound $LB = \boldsymbol{c}^{\mathrm{T}}\boldsymbol{x}^*_n + \eta^*_n$.

Step 3: Solve sub-problem (36)–(37) to obtain the solution $\boldsymbol{y}^*_n$ to operational decisions and update the upper bound UB.

Step 4: If $UB - LB \le \varphi$, then stop and output the results. Otherwise, go back to Step 2.

B. Distributed ATC Algorithm

The distributed algorithm is an effective approach to solving the coordinated planning problem of the entire power grid. By communicating the variables of power flow on the tie lines, the algorithm can obtain the planning scheme while minimizing the cost of information exchange. This approach also ensures the privacy of regional power grid information.

Considering that the ATC algorithm is easily extendable to parallel computing, it has been adopted to solve multi-regional planning problems. The ATC algorithm allows the individual regions to solve their planning problems separately and then exchange the variables of power flow on the tie lines. This process is repeated until the convergence conditions (40)–(41) are met. It is worthwhile to mention that this algorithm can enable parallel computing and reduce computational complexity, leading to higher computational efficiency.

Taking the case in Fig. 3 as an example, with the ATC algorithm, the Lagrange penalty function is applied to relax the coupling constraint (5). The objectives of Region A and Region B can be respectively formulated as in (38) and (39), where $\boldsymbol{\lambda}_{ij}$ is Lagrange multiplier and $\boldsymbol{\mu}_{ij}$ represents a quadratic penalty factor. They are utilized to ensure solution optimality and facilitate algorithm convergence. The operator $\circ$ represents the Hamilton multiplier.

$$\min C_A = C + \sum_{s\in S} D_s[(\boldsymbol{\lambda}_{ij})^{\mathrm{T}}(\boldsymbol{P}^A_{s,i} - \boldsymbol{P}^B_{s,j}) + \|\boldsymbol{\mu}_{ij}\circ(\boldsymbol{P}^A_{s,i} - \boldsymbol{P}^B_{s,j})\|^2_2] \tag{38}$$

$$\min C_B = C + \sum_{s\in S} D_s[(\boldsymbol{\lambda}_{ij})^{\mathrm{T}}(\boldsymbol{P}^A_{s,i} - \boldsymbol{P}^B_{s,j}) + \|\boldsymbol{\mu}_{ij}\circ(\boldsymbol{P}^A_{s,i} - \boldsymbol{P}^B_{s,j})\|^2_2] \tag{39}$$

The convergence condition of the ATC algorithm is:

$$\Delta P = \|\boldsymbol{P}^A_i - \boldsymbol{P}^B_j\|_2 \le \varepsilon_1 \tag{40}$$

$$\Delta C = \frac{|(C^k_A - C^k_B) - (C^{k-1}_A - C^{k-1}_B)|}{C^k_A - C^k_B} \le \varepsilon_2 \tag{41}$$

The flowchart of the iterative solving process is shown in Fig. 4. The process of the ATC algorithm is as follows:

Step 1: Initialize the number of iterations $k = 0$; the convergence error ε_1 and ε_2; Lagrange multiplier λ; quadratic penalty factor μ; and the initial value to the variables of power flow on the tie lines, namely $\boldsymbol{P}^A_j$ and $\boldsymbol{P}^B_j$.

Step 2: Solve the planning problem of Region B, and communicate the obtained optimal value of $\boldsymbol{P}^B_j$ to Region A.

Step 3: Solve the planning problem of Region A and obtain the optimal value to variable $\boldsymbol{P}^A_i$.

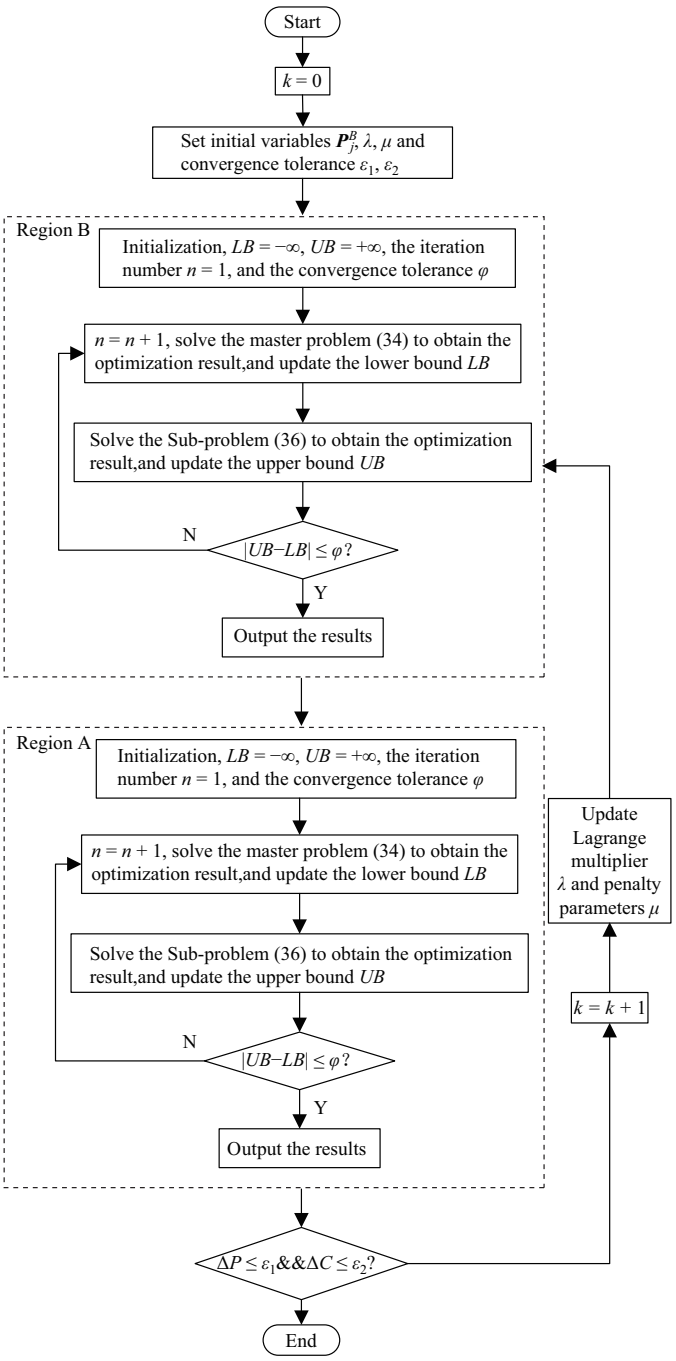

Fig. 4. The flowchart of the iterative solving process.

Step 4: If the convergence condition is satisfied, i.e., $\Delta P \leq \varepsilon_1$ and $\Delta C \leq \varepsilon_2$, terminate and output the result; otherwise go to step 5.

Step 5: Set $k = k + 1$. Communicate $\boldsymbol{P}_i^A$ to Region B. Update the Lagrange multiplier λ and the quadratic penalty factor μ according to (42), and then go to **step 2**. In (42), γ is set as 2.

$$\begin{cases} \lambda_{ij,k+1} = \lambda_{ij,k} + 2\boldsymbol{\mu}_{ij,k} \circ \boldsymbol{\mu}_{ij,k} \circ (\boldsymbol{P}_i^A - \boldsymbol{P}_j^B) \\ \boldsymbol{\mu}_{ij,k+1} = \gamma \boldsymbol{\mu}_{ij,k} \quad 2 \leq \gamma \leq 3 \end{cases} \tag{42}$$

C. Convergence and Optimality of the ATC Algorithm

According to the model described in Section III, it can be rewritten as follows:

$$\begin{cases} \min\limits_{x} f(x) \\ \text{s.t.} \;\; g(x) \leq 0, h(x) = 0 \end{cases} \tag{43}$$

where x is a vector of independent and dependent variables. The first term of the constraint represents (8)–(9), (11)–(25), (28), (32)–(33), the second term represents (10), (26)–(27), (30)–(31). Define the integers p^I and p^E to be the number of inequality and equality constraints, respectively. n is the number of rows of the variable vector of equation (43). Let I_n be the n-row identity matrix.

With the ATC algorithm, the planning problem of Region A can be rewritten in the following form:

$$\begin{cases} \min\limits_{x} f(x) \\ \text{s.t.} \;\; g(x) \leq 0, h(x) = 0, F_A x = d_A \end{cases} \tag{44}$$

where F_A is a submatrix that consists of the first n_A rows of the identity matrix I_n and d_A is a parameter from the planning subproblem of Region B. Define the integers p_A^I and p_A^E to be the number of inequalities and equality constraints in region A involving only variable x. Similarly, the planning problem for Region B can also be written as:

$$\begin{cases} \min\limits_{x} f(x) \\ \text{s.t.} \;\; g(x) \leq 0, h(x) = 0, F_B x = d_B \end{cases} \tag{45}$$

where F_B is a submatrix that consists of the last n_B rows of the identity matrix I_n, and d_B is the parameter from Region A. Define the integers p_B^I and p_B^E to be the number of inequalities and equality constraints in region B involving only variable x.

Let $J(x)$ be the $(p^I + p^E) \times n$ matrix $[J^I(x); J^E(x)]$ where $J^I(x)$ and $J^E(x)$ are the Jacobians of $g(x)$ and $h(x)$. This matrix function $J(x)$ will be called the Jacobian of (43).

For a fixed point x^*, define $T_a(x^*)$ to be the set of the indices corresponding to the active inequality constraints at x^*:

$$T_a(x^*) := \{i \mid g_i(x^*) = 0\} \tag{46}$$

where g_i denotes the i-th inequality constraint.

Define an integer p_a^I to be the number of inequality constraints at x^*. The integers $p_{a,A}^I$ and $p_{a,B}^I$ are the number of inequality constraints in regions A and B involving only the variable x. Reference [41] shows that $p_a^I = p_{a,A}^I + p_{a,B}^I$. Let a $p_a^I \times n$ matrix $J_a^I(x^*)$ be the submatrix of $J^I(x^*)$ consisting of the active inequality constraints at x^*.

We consider that x^* is an accumulation point of the ATC process. As it is the solution for problems (44) and (45), there exist vectors $z^I \geq 0$, z^E, and u, and vectors $w^I \geq 0$, w^E and v such that the following two equations hold simultaneously:

$$\begin{cases} -\nabla f(x^*) = J_a^I(x^*)^t z^I + J^E(x^*)^t z^E + F_A u \\ -\nabla f(x^*) = J_a^I(x^*)^t w^I + J^E(x^*)^t w^E + F_B v \end{cases} \tag{47}$$

The Lagrange multiplier theorem states that a regular point x^* is a solution to a multi-regional planning model, if and

only if there exists a nonnegative vector λ^I and a vector λ^E such that:

$$\nabla f(x^*) + J_a^I(x^*)^t \lambda^I + J_a^E(x^*)^t \lambda^E = 0 \tag{48}$$

Reference [41] shows that for some vectors $\lambda^I \geq 0$ and λ^E, if equation (45) is satisfied, then x^* automatically satisfies equation (46), which proves that the ATC algorithm converges to the global optimal solution.

V. Case Studies

To evaluate the effectiveness of the proposed model and the solving algorithm, a 48-bus test system composed of two modified IEEE 24-bus systems [42] is used. With Matlab 2021a, Yalmip toolbox and Gurobi are used to build and solve the model.

A. System settings

The test system is shown in Fig. 5. The two modified IEEE 24-bus systems have identical structures but different parameters and scenario designs. The maximum output of thermal units in Region A and Region B is increased by 1.6 times based on the original settings. Additionally, 1000 MW wind farms are added to buses 2, 7, and 19 of Regions A and Region B. The coal-fired units at buses 1, 2, and 16 in Region A and buses 1, 15, 16, and 21 in Region B are replaced by gas-fired units. The total maximum loads of the two regions are increased by 2.2 and 1.9 times, respectively. The capacities of all lines are reduced to 85% of their original values.

The candidate ESS installation locations, maximum capacities, and other relevant parameters are listed in Table I. The cost coefficient of ESS investment is 20 \$/kWh and 500 \$/kW [43]. This paper considers a static planning model with an annual interest rate of 10%. The lifetime of the ESS and transmission line is 10 years and 50 years, respectively, with no residual value. The investment costs of transmission lines are set in reference [44]. The wind curtailment penalty is 500 \$/MWh, and the carbon emission quota factor (η), is set to 0.798 tCO_2/MWh. The base price carbon emission quota is $c_{CO_2} = 25\$$. The amount of each carbon emission quota tier is set as $L_1 = 40$ t, and the price growth coefficient is set as $\tau_1 = 0.25$.

Scenario generation and reduction is to obtain a set of representative and diverse scenarios through random sampling

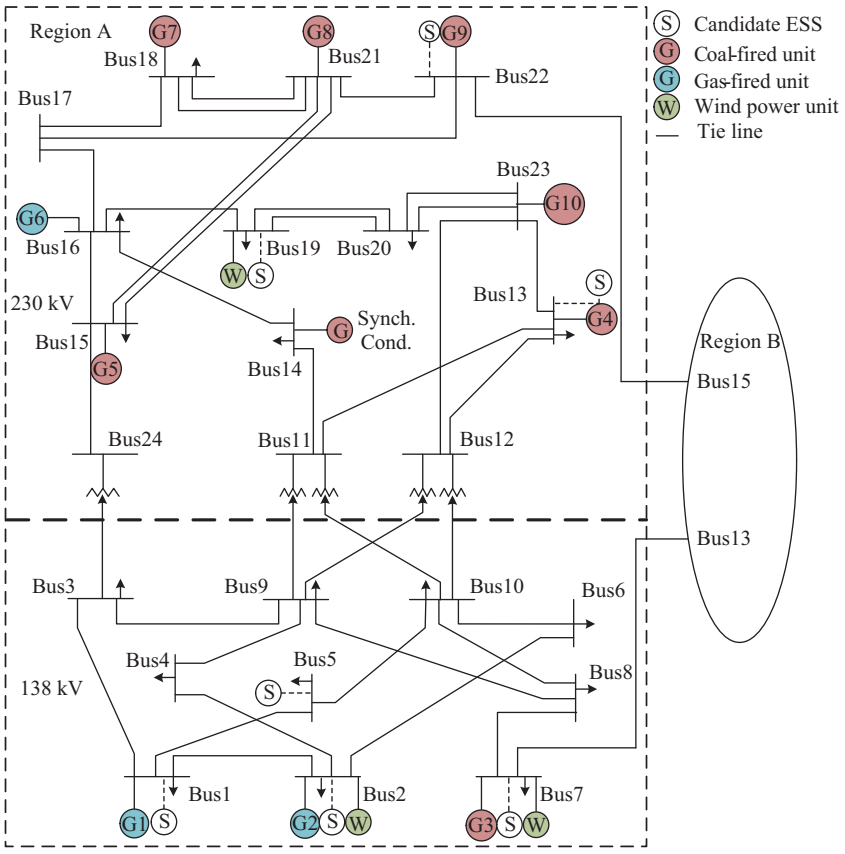

Fig. 5. The modified two-regional IEEE-48 bus test system.

TABLE I
ENERGY STORAGE SYSTEM PARAMETERS

Bus number	Maximum capacity (MW)	Maximum energy (MWh)	Initial energy rate	Charging/discharging rate	Self-discharge rate	Energy-to-power time (h)
1, 2, 5, 7, 13, 19, 22	100	400	20%	90%	0.2%	4

and screening of uncertainty factors to analyze and optimize the operating status of the power system, which is crucial for stochastic programming. In this study, we utilize the K-means clustering method to merge the data of 365 days from reference [45] into three representative days as shown in Fig. 6. They capture the actual operation scenarios of renewable energy and load demands.

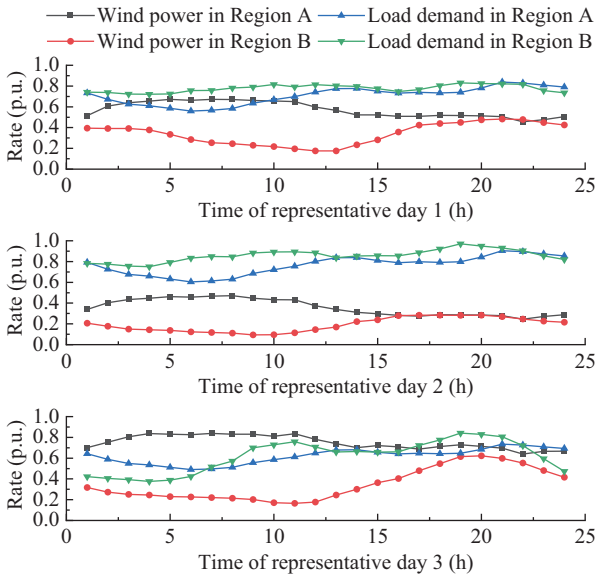

Fig. 6. The proportion of renewable energy generation and load demand.

The two regions are connected through two tie lines, i.e., A22-B15 (bus 22 of region A and bus 15 of region B) and A7-B13 (bus 7 of region A and bus 13 of region B). The maximum transmission capacities of the two tie lines are set to 200 MW. For the ATC algorithm, the convergence error is set as $\varepsilon_1 = \varepsilon_2 = 10^{-3}$; the Lagrange multiplier is initialized as $\lambda_{ij} = 0$; the quadratic penalty factor is set as $\mu_{ij} = 1$; and the initial power flows on the tie lines are set as $\boldsymbol{P}_i^A = \mathbf{0}$.

Four different cases are tested for comparative analysis:

Case 1: ESS Planning and carbon emission quota trading.

Case 2: ESS Planning only.

Case 3: Carbon emission quota trading only.

Case 4: ESS Planning and carbon emission quota trading; Isolated Region A and Region B, i.e., no tie-lines connecting the two regions.

B. Comparison of different planning cases

The iterative calculation process of the total cost and some shared variables of Case 1 is shown in Fig. 7. The fourth iteration outputs a solution close to the final solution. The iterative process converges at the eighth iteration, i.e., satisfies the convergence conditions ε_1 and ε_2.

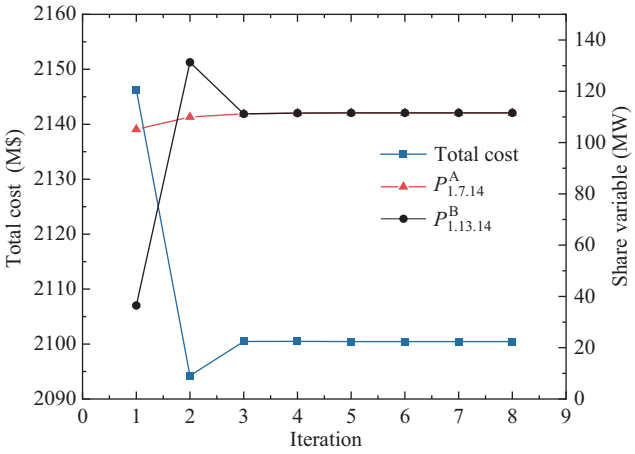

Fig. 7. The convergence process of the ATC algorithm.

To validate the effectiveness of the ATC algorithm, a comparison between the distributed and centralized solution methods is conducted. The results of the four cases in this paper are presented in Tables II and III.

It can be seen from Table III, that the gap in total costs with the distributed algorithm compared to the centralized method is tiny. The maximum gap in the four cases is merely 0.88%, which means that the distributed algorithm can achieve comparable optimality to the centralized method.

Among the four cases, Case 1 shows the lowest total cost of 2100.47 M$, highlighting the economic benefit and carbon emission reduction brought by ESSs and carbon emission quota trading.

TABLE II
PLANNING RESULTS FOR FOUR CASES

Case number	Line		ESS			
			Total energy (MWh)		Total capacity (MW)	
	RA	RB	RA	RB	RA	RB
1	1–2, 1–5, 7–8, 14–16, 16–19	1–2, 1–5, 7–8, 16–19	663	216	102	36
2	1–2, 7–8, 14–16, 16–19	1–2, 2–6, 7–8, 16–19	885	216	150	36
3	1–2, 1–5, 2–4, 7–8, 16–19	1–2, 1–5, 7–8, 16–19	–	–	–	–
4	1–2, 1–5, 7–8, 14–16, 16–19	1–2, 1–5, 7–8, 16–19	662	216	120	36

TABLE III
THE VARIOUS COSTS OF THE FOUR CASES

Case number	Investment cost (M$)	Generation cost (M$)	Wind curtailment cost (M$)	CETC (M$)	Total cost (M$)	Cen-total cost (M$)	Gap
1	29.66	1434.56	128.12	508.13	2100.47	2090.76	0.46%
2	34.83	1378.15	128.12	782.77	2323.87	2339.92	0.69%
3	20.38	1444.06	189.59	504.54	2158.57	2139.84	0.88%
4	30.98	1490.47	728.57	335.23	2583.92	2583.92	0.00%

From Table II, the planning results of the four cases show obvious differences in transmission expansion planning schemes for Region A and Region B. This is mainly because Region A has abundant and fluctuating wind energy resources, requiring a more power-carrying transmission network and more ESSs to effectively accommodate wind energy. In contrast, Region B has less wind energy, and thus needs a lower transmission capacity and fewer ESSs. In sum, both regions expand transmission lines from buses 1, 7, and 19, highlighting the importance of transmission line expansion in reducing congestion and improving wind power consumption.

Comparing Case 1 and Case 2, it can be seen that in Case 1 for Region A and B lines 1–5 are planned, while in in Case 2, only in Region A lines 1–5 is planned and in region B lines 2–6 is planned instead. This difference is caused by the increase in maximum power and capacity of the ESS at bus 2 in Region A, and the addition of a new energy storage system at bus 5 in Case 2. By adding ESSs, Case 2 achieves a more balanced energy supply and demand, reducing the need for line expansion in Region A. Furthermore, Case 1 considers carbon emissions trading, which leads to the output increase of unit G1 in both regions. This also enhances the need for line expansion to avoid transmission congestion.

Compared to Case 1, the transmission expansion plan in Region A changed from lines 14–16 to 2–4 in Case 3. This is because Case 1 had a new energy storage system (20 MW/263 MWh) installed at bus 2, while Case 3 did not utilize energy storage systems. Thus, Case 3 could only reduce carbon emissions by modifying the transmission line expansion plan and introducing additional power from G2 and wind power into the system.

In Case 4, the inter-regional connection was not considered. As a result, the curtailed wind power in the system increased, leading to a higher proportion of curtailed wind power cost. Compared to Case 1, the line expansion plan remained the same. However, to minimize wind curtailment, the capacity of the energy storage system in Region A significantly increased from 102 MW to 120 MW while its energy remained the same. The system expansion remained unchanged in Region B, where wind power fluctuations are small.

C. Sensitivity to different parameters

1) Impact of Carbon Emission Trading Mechanism

The comparison between Case 1 and Case 2 indicates that Case 1 has a lower investment cost and a lower cost on carbon emission quota trading but a higher generation cost than Case 2. Overall, the total cost of Case 1 is lower than that of Case 2 by 223.4 M$. The main reasons for the difference between the generation costs of the two cases are caused by carbon emission trading as shown in Table III as well as the typical daily output of each unit as shown in Fig. 8. When considering the cost of carbon emission quota trading, the output of gas-fired units with lower carbon emissions significantly increases. In comparison, the output of coal-fired units with higher carbon emissions decreases to the lowest level. Although gas-fired units have lower carbon emissions per unit of electricity, their generation costs are higher than that of coal-fired units. Therefore, the generation cost in Case 1 is higher than that

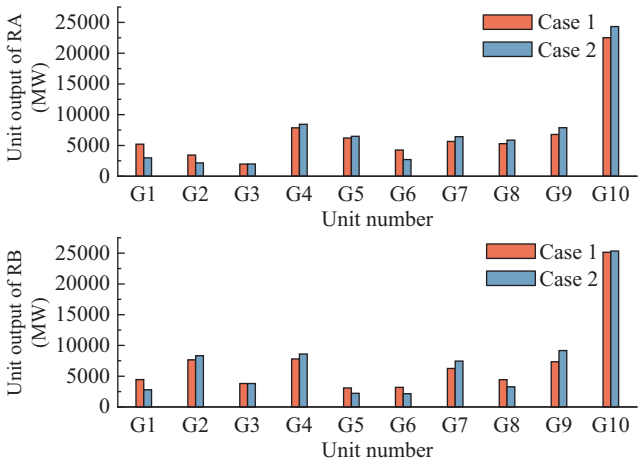

Fig. 8. Outputs of the units in the two regions on a typical day.

in Case 2. This shows the importance of considering carbon emission quota trading, as it can lead to different decisions on unit scheduling, which could further affect the decisions on transmission expansion.

2) Impact of ESS and Tie-line Capacity on Wind Power Curtailment

To quantify the accommodation of renewable energy, wind energy curtailment rates are calculated for different scenarios, as shown in (49). As shown in Fig. 9, when ESS is not considered (i.e., Case 3), the wind energy curtailment rate is 1.6%. Compared to Case 1, Case 3 exhibits a smaller variation in wind curtailment rate. This is caused by the limitation imposed by the capacity of the ESS and shows the role of the energy storage system in accommodating renewable energy.

$$\mathrm{WCR} = \frac{\sum_{t\in T}\sum_{w\in W}(P_{s,w}^{\max} - P_{s,w,t})\Delta t}{\sum_{t\in T}\sum_{w\in W}P_{s,w}^{\max}\Delta t} \times 100\% \quad (49)$$

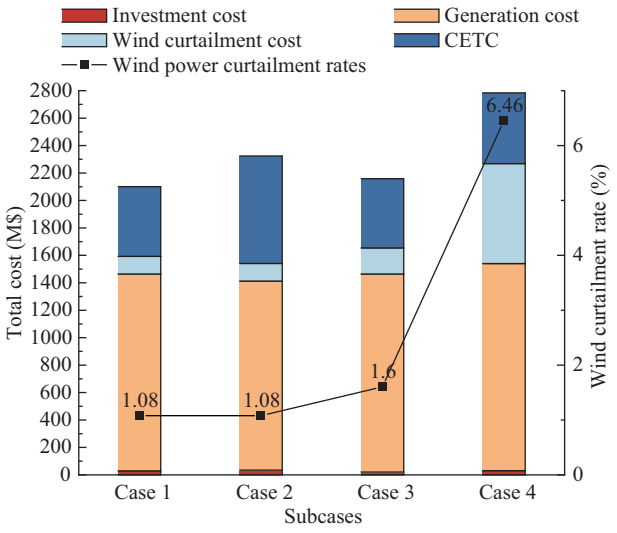

Fig. 9. Cost and wind curtailment rates of the four cases.

Due to the capacity limitations of the tie-lines, the transmission of power between regions is restricted, affecting the multi-regional system's ability to achieve a better objective. A

sensitivity study is conducted to explore the impact of the tie-line capacities on the total cost and wind energy curtailment. The capacities of the tie-lines are set from 0 MW to 300 MW with a step of 50 MW, as shown in Fig. 10. The increasing tie-line capacity not only reduces the operation cost but also promotes the accommodation of wind energy in interconnected regions. The operational cost decreased from 2752.84 M$ to 1997.04 M$, resulting in a saving of 755.80 M$. The curtailment rate decreased from 6.46% to 0.53%. Notably, no further improvement is observed when the tie-line capacity reaches 300 MW. This suggests that planning tie-lines with appropriate transmission capacities based on the grid situation can improve the accommodation of renewable energy in the multi-regional power system.

3) Impact of Carbon Emission Quota Price on Carbon Emissions and Unit Scheduling

Different carbon emission quota base prices can lead to different optimal carbon emission quota demands. Fig. 11 illustrates the changes in carbon emissions and generation costs associated with varying carbon emission quota base prices. When the base price increases, carbon emissions decrease gradually. This is because, at low CET base prices, the carbon

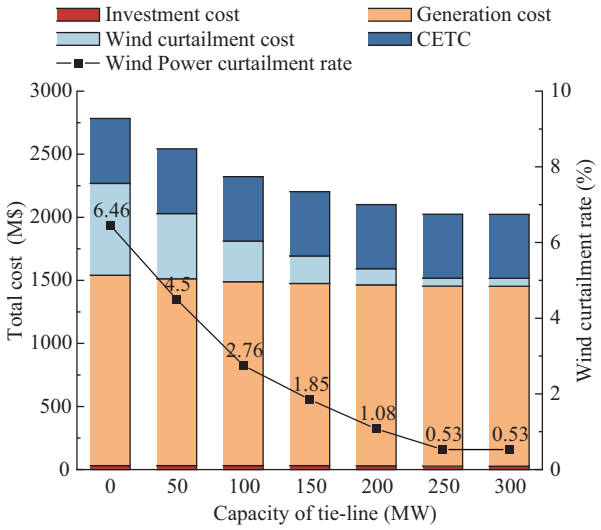

Fig. 10. Cost and wind curtailment rate with different tie-line capacities.

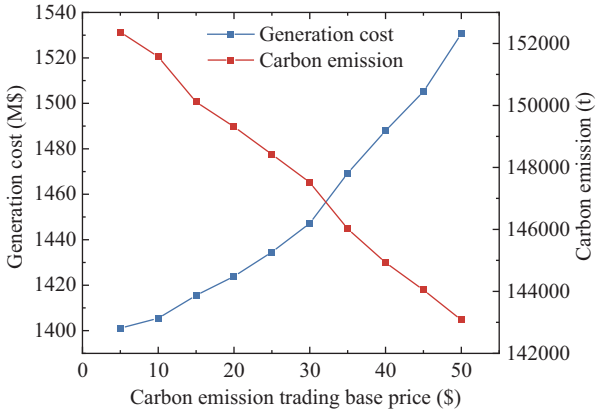

Fig. 11. Carbon emissions and generation costs under various carbon emissions trading prices.

emission quota trading cost represents a small proportion of the total cost. However, as CET base prices rise, the proportion of CETC in the total cost increases, leading to greater output from gas-fired units, which are more environmentally friendly than coal-fired units but have higher generation costs. As a result, generation costs show an upward trend. When the CET base price reaches a sufficiently high level, each gas-fired unit will operate at full power, leading to the minimum possible carbon emissions.

4) Efficiency Analysis of Various Solving Algorithms

To highlight the advantages of the C&CG algorithm employed in this paper, a comparative study was conducted with commonly used methods for solving mixed-integer programming models, including Benders [46] and branch-and-bound [47] algorithms. The results are shown in Table IV. By comparing the solution times of four different cases, we can observe the significant advantages of the C&CG algorithm in terms of solution speed, especially in the most complex Case 1. This advantage is particularly significant. Compared with Benders, the calculation time of C&CG is reduced by 23.95%, and compared with branch and bound, the calculation time is reduced by 44.01%. This shows that the C&CG algorithm has obvious efficiency and performance advantages in dealing with the problems proposed in this paper.

TABLE IV
SOLUTION EFFICIENCY COMPARISONS FOR DIFFERENT ALGORITHMS

Case number	C&CG	Benders	Branch and bound
1	327 s	430 s	584 s
2	284 s	339 s	435 s
3	185 s	235 s	302 s
4	94 s	111 s	148 s

VI. CONCLUSION

This paper has proposed a planning model for interconnected multi-regional power considering ESS planning, transmission expansion, and carbon emission quota trading. It also employs the ATC algorithm to solve the model in a distributed manner. The conclusions drawn from the case analysis are as follows:

1) Integrating carbon emission trading into the planning problem can effectively help reduce the total cost and promote collaborative optimization of a low-carbon economy.

2) The carbon emission quota base price can significantly impact the planning result. Therefore, a reasonable carbon emission quota base price based on the actual situation is essential to balance carbon reduction and economic efficiency.

3) Jointly considering ESS planning and transmission expansion is essential to improving wind energy accommodation.

In this paper, the carbon quota is determined using the baseline method, which has certain limitations. In the future, we will investigate the allocation methods for carbon emissions quotas in cross-regional carbon trading mechanisms.

REFERENCES

[1] D. S. Mallapragada, N. A. Sepulveda, and J. D. Jenkins, "Long-run system value of battery energy storage in future grids with increasing wind and solar generation," *Applied Energy*, vol. 275, pp. 115390, Oct. 2020.

[2] W. H. Zhang, D. Y. Rui, W. H. Wang, Y. Guo, Z. X. Jing, and W. H. Tang, "Cyber-physical resilience enhancement for power transmission systems with energy storage systems," *CSEE Journal of Power and Energy Systems*, vol. 10, no. 2, pp. 844–855, Dec. 2023.

[3] J. Liu, P. L. Zeng, H. Xing, Y. L. Li, and Q. W. Wu, "Optimal operation of flexible distribution networks for security improvement considering active management," *CSEE Journal of Power and Energy Systems*, vol. 9, no. 3, pp. 996–1007, May 2023.

[4] X. Y. Chen, L. Bu, C. Chen, L. Gan, and K. Yu, "An operational optimization method of regional multi-energy system considering thermal quasi-dynamic characteristics," *CSEE Journal of Power and Energy Systems*, vol. 10, no. 6, pp. 2551–2563, Nov. 2024.

[5] X. L. Liu, Y. B. Liu, J. Y. Liu, Y. Xiang, and X. D. Yuan, "Optimal planning of AC-DC hybrid transmission and distributed energy resource system: review and prospects," *CSEE Journal of Power and Energy Systems*, vol. 5, no. 3, pp. 409–422, Sep. 2019.

[6] A. K. Kazerooni and J. Mutale, "Transmission network planning under security and environmental constraints," *IEEE Transactions on Power Systems*, vol. 25, no. 2, pp. 1169–1178, May 2010.

[7] H. Zhang and B. Zhang, "The unintended impact of carbon trading of China's power sector," *Energy Policy*, vol. 147, pp. 111876, Dec. 2020.

[8] Y. J. Xian, K. Wang, Y. M. Wei, and Z. M. Huang, "Would China's power industry benefit from nationwide carbon emission permit trading? An optimization model-based ex post analysis on abatement cost savings," *Applied Energy*, vol. 235, pp. 978–986, Feb. 2019.

[9] F. Yu, X. D. Chu, D. L. Sun, and X. M. Liu, "Low-carbon economic dispatch strategy for renewable integrated power system incorporating carbon capture and storage technology," *Energy Reports*, vol. 8, no. S10, pp. 251–258, Nov. 2022.

[10] R. F. Zhang, T. Jiang, L. Q. Bai, G. Q. Li, H. H. Chen, X. Li, and F. X. Li, "Adjustable robust power dispatch with combined wind-storage system and carbon capture power plants under low-carbon economy," *International Journal of Electrical Power & Energy Systems*, vol. 113, pp. 772–781, Dec. 2019.

[11] C. Yang, J. J. Liu, H. X. Liao, G. Q. Liang, and J. H. Zhao, "An improved carbon emission flow method for the power grid with prosumers," *Energy Reports*, vol. 9, pp. 114–121, Dec. 2023.

[12] Y. W. Wu, S. H. Lou, and S. Y. Lu, "A model for power system interconnection planning under low-carbon economy with CO_2 emission constraints," *IEEE Transactions on Sustainable Energy*, vol. 2, no. 3, pp. 205–214, Jul. 2011.

[13] B. W. Li, Y. H. Song, and Z. C. Hu, "Carbon flow tracing method for assessment of demand side carbon emissions obligation," *IEEE Transactions on Sustainable Energy*, vol. 4, no. 4, pp. 1100–1107, Oct. 2013.

[14] J. F. Li, X. T. He, W. D. Li, M. Z. Zhang, and J. Wu, "Low-carbon optimal learning scheduling of the power system based on carbon capture system and carbon emission flow theory," *Electric Power Systems Research*, vol. 218, pp. 109215, May 2023.

[15] X. H. Zhang, K. Tomsovic, and A. Dimitrovski, "Security constrained multi-stage transmission expansion planning considering a continuously variable series reactor," *IEEE Transactions on Power Systems*, vol. 32, no. 6, pp. 4442–4450, Nov. 2017.

[16] J. Qiu, Z. Y. Dong, J. H. Zhao, K. Meng, F. J. Luo, K. P. Wong, and C. Lu, "A low-carbon oriented probabilistic approach for transmission expansion planning," *Journal of Modern Power Systems and Clean Energy*, vol. 3, no. 1, pp. 14–23, Mar. 2015.

[17] Q. X. Chen, C. Q. Kang, Q. Xia, and J. Zhong, "Power generation expansion planning model towards low-carbon economy and its application in China," *IEEE Transactions on Power Systems*, vol. 25, no. 2, pp. 1117–1125, May 2010.

[18] J. L. Jin, X. Y. Zhang, L. L. Xu, Q. L. Wen, and X. J. Guo, "Impacts of carbon trading and wind power integration on carbon emission in the power dispatching process," *Energy Reports*, vol. 7, pp. 3887–3897, Nov. 2021.

[19] R. F. Zhang, H. H. Chen, X. Li, T. Jiang, G. Q. Li, and R. X. Ning, "Low-carbon economic dispatch model with combined wind-storage system and carbon capture power plants," in *2017 IEEE Power & Energy Society General Meeting*, 2017, pp. 1–5.

[20] M. S. Lu, C. L. Chang, W. J. Lee, and L. Wang, "Combining the wind power generation system with energy storage equipment," *IEEE Transactions on Industry Applications*, vol. 45, no. 6, pp. 2109–2115, Nov./Dec. 2009.

[21] M. Dicorato, G. Forte, M. Pisani, and M. Trovato, "Planning and operating combined wind-storage system in electricity market," *IEEE Transactions on Sustainable Energy*, vol. 3, no. 2, pp. 209–217, Apr. 2012.

[22] A. J. Conejo, Y. H. Cheng, N. Zhang, and C. Q. Kang, "Long-term coordination of transmission and storage to integrate wind power," *CSEE Journal of Power and Energy Systems*, vol. 3, no. 1, pp. 36–43, Mar. 2017.

[23] S. Dehghan and N. Amjady, "Robust transmission and energy storage expansion planning in wind farm-integrated power systems considering transmission switching," *IEEE Transactions on Sustainable Energy*, vol. 7, no. 2, pp. 765–774, Apr. 2016.

[24] X. Zhang and A. J. Conejo, "Coordinated investment in transmission and storage systems representing long- and short-term uncertainty," *IEEE Transactions on Power Systems*, vol. 33, no. 6, pp. 7143–7151, Nov. 2018.

[25] J. Lee, J. H. Kim, and S. K. Joo, "Stochastic method for the operation of a power system with wind generators and superconducting magnetic energy storages (SMESs)," *IEEE Transactions on Applied Superconductivity*, vol. 21, no. 3, pp. 2144–2148, Jun. 2011.

[26] A. Bytyqi, S. Gandhi, E. Lambert, and N. Petrovič, "A review on TSO-DSO data exchange, CIM extensions and interoperability aspects," *Journal of Modern Power Systems and Clean Energy*, vol. 10, no. 2, pp. 309–315, Mar. 2022.

[27] T. Erseghe, "Distributed optimal power flow using ADMM," *IEEE Transactions on Power Systems*, vol. 29, no. 5, pp. 2370–2380, Sep. 2014.

[28] T. Erseghe, "A distributed and scalable processing method based upon ADMM," *IEEE Signal Processing Letters*, vol. 19, no. 9, pp. 563–566, Sep. 2012.

[29] H. Du, T. Lin, Q. Y. Li, X. Y. Fu, and X. L. Xu, "Decentralized optimal power flow based on auxiliary problem principle with an adaptive core," *Energy Reports*, vol. 8, no. S13, pp. 755–765, Nov. 2022.

[30] M. Alkhraijah, M. Alowaifeer, S. Grijalva, and D. K. Molzahn, "Distributed multi-period DCOPF via an auxiliary principle problem algorithm," in *2021 IEEE Texas Power and Energy Conference (TPEC)*, 2021, pp. 1–6.

[31] A. Kargarian, M. Mehrtash, and B. Falahati, "Decentralized implementation of unit commitment with analytical target cascading: a parallel approach," *IEEE Transactions on Power Systems*, vol. 33, no. 4, pp. 3981–3993, Jul. 2018.

[32] J. Liu, H. Z. Cheng, P. L. Zeng, L. Z. Yao, C. Shang, and Y. Tian, "Decentralized stochastic optimization based planning of integrated transmission and distribution networks with distributed generation penetration," *Applied Energy*, vol. 220, pp. 800–813, Jun. 2018.

[33] S. DorMohammadi and M. Rais-Rohani, "Exponential penalty function formulation for multilevel optimization using the analytical target cascading framework," *Structural and Multidisciplinary Optimization*, vol. 47, no. 4, pp. 599–612, Jan. 2013.

[34] M. Mehrtash, A. Kargarian, and A. Mohammadi, "Distributed optimisation-based collaborative security-constrained transmission expansion planning for multi-regional systems," *IET Generation, Transmission & Distribution*, vol. 13, no. 13, pp. 2819–2827, Jul. 2019.

[35] R. F. Zhang, K. F. Yan, G. Q. Li, T. Jiang, X. Li, and H. H. Chen, "Privacy-preserving decentralized power system economic dispatch considering carbon capture power plants and carbon emission trading scheme via over-relaxed ADMM," *International Journal of Electrical Power & Energy Systems*, vol. 121, pp. 106094, Oct. 2020.

[36] H. W. Zhong, G. L. Zhang, Z. F. Tan, G. C. Ruan, and X. Wang, "Hierarchical collaborative expansion planning for transmission and distribution networks considering transmission cost allocation," *Applied Energy*, vol. 307, pp. 118147, Feb. 2022.

[37] J. Liu, Z. Tang, P. P. Zeng, Y. L. Li, and Q. W. Wu, "Distributed adaptive expansion approach for transmission and distribution networks incorporating source-contingency-load uncertainties," *International Journal of Electrical Power & Energy Systems*, vol. 136, pp. 107711, Mar. 2022.

[38] C. M. Zhang, H. Z. Cheng, L. Liu, H. Zhang, X. H. Zhang, and G. Li, "Coordination planning of wind farm, energy storage and transmission network with high-penetration renewable energy," *International Journal of Electrical Power & Energy Systems*, vol. 120, pp. 105944, Sep. 2020.

[39] Ministry of Ecology and Environment of the People's Republic of China. (2022, Oct.). 2021 and 2022 national carbon emissions trading allowance setting and allocation implementation plan. [Online]. Available: https://www.mee.gov.cn/xxgk2018/xxgk/xxgk06/202211/W020221103336161991455.pdf.

[40] J. Liu, Z. Tang, P. P. Zeng, Y. L. Li, and Q. W. Wu, "Fully distributed second-order cone programming model for expansion in transmission and distribution networks," *IEEE Systems Journal*, vol. 16, no. 4, pp. 6681–6692, Dec. 2022.

[41] N. Michelena, H. Park, and P. Y. Papalambros, "Convergence properties

of analytical target cascading," *AIAA Journal*, vol. 41, no. 5, pp. 897–905, May 2003.
[42] J. Liu, P. P. Zeng, H. Xing, Y. L. Li, and Q. W. Wu, "Hierarchical duality-based planning of transmission networks coordinating active distribution network operation," *Energy*, vol. 213, pp. 118488, Dec. 2020.
[43] H. Pandžić, Y. S. Wang, T. Qiu, Y. Dvorkin, and D. S. Kirschen, "Near-optimal method for siting and sizing of distributed storage in a transmission network," *IEEE Transactions on Power Systems*, vol. 30, no. 5, pp. 2288–2300, Sep. 2015.
[44] N. Alguacil, A. L. Motto, and A. J. Conejo, "Transmission expansion planning: a mixed-integer LP approach," *IEEE Transactions on Power Systems*, vol. 18, no. 3, pp. 1070–1077, Aug. 2003.
[45] J. Liu, Z. Tang, M. J. Yu, P. Z. Ren, P. L. Zeng, and W. J. Jia, "Robust expansion planning model of integrated energy system with energy hubs integrated," *Electric Power Systems Research*, vol. 226, pp. 109947, Jan. 2024.
[46] J. P. Wang, P. L. Zeng, J. X. Fan, B. Jiang, and G. J. Ma, "Stochastic expansion planning of integrated energy system: a benders-based decomposition approach," *Energy Reports*, vol. 9, no. S10, pp. 794–804, Oct. 2023.
[47] C. F. Wang, Y. Q. Bai, and P. P. Shen, "A practicable branch-and-bound algorithm for globally solving linear multiplicative programming," *Optimization*, vol. 66, no. 3, pp. 397–405, Jan. 2017.

Jia Liu received the B.S. and Ph.D. degrees in Electrical Engineering from Tianjin University, Tianjin, China, and Shanghai Jiao Tong University, Shanghai, China, in 2014 and 2019, respectively. He was a postdoctoral and visiting scholar with Zhejiang University, Hangzhou, China, and Cardiff University, Cardiff, U.K., during 2020–2022 and 2023–2024, respectively. He is currently an Associate Professor in Hangzhou Dianzi University, Hangzhou, China. He is the secretary-general of IEEE PES China Education Committee. His main research interests are planning, assessment and operation of power and energy systems, distributed optimization in transmission and distribution networks.

Biao Jiang received the B.S. and M.S. degrees in Electrical Engineering from Shanghai Dianji University, Shanghai, China, and Hangzhou Dianzi University, Hangzhou, China, in 2021 and 2024, respectively. He is currently an engineer in GoodWe Technologies Co., Ltd., Suzhou, China. His main research interest is transmission network low-carbon planning.

Zao Tang received the B.S. and Ph.D. degrees from the College of Electrical Engineering, Sichuan University, Chengdu, China, in 2016 and 2021, respectively. She was a Visiting Scholar with the Stevens Institute of Technology, Hoboken, NJ, USA, during 2019–2020. She is currently a Research Lecture with the Department of Automation, Hangzhou Dianzi University, Hangzhou, China. Her research interests include the optimal planning and operation of power systems.

Pingliang Zeng received the B.S. and Ph.D. degrees in Electrical Engineering from Huazhong University of Science and Technology, China, and Strathclyde University, U.K., in 1984 and 1990, respectively. He is currently a Professor in Hangzhou Dianzi University, Hangzhou, China. His current research interests are power system planning, integration of energy storage in low carbon electricity systems.

Tong Su received the B.Sc. and M.S. degrees in Electrical Engineering from Sichuan University, Chengdu, China, in 2019 and 2022, respectively. Since 2022, he has been working toward the Ph.D. degree from the University of Connecticut, Storrs, CT, USA. His research interests include power system dynamics and stability control with inverter-based resources, machine learning and optimization.

Yalou Li received the B.S. degree in Electrical Engineering from Huazhong University of Science and Technology, Wuhan, China, in 1997. In 2000 and 2003, he received M.S. and Ph.D. degrees respectively in electrical engineering from the China Electric Power Research Institute, Beijing, China, where he is currently a Chief Engineer. His main research interests are key devices digital simulation, analysis and control.

Qiuwei Wu received the Ph.D. degree in Power System Engineering from Nanyang Technological University, Singapore, in 2009. He has been working at the Department of Electrical Engineering, Technical University of Denmark (DTU) since Nov. 2009. His research interests are operations and control of power systems with high penetration of renewables, including wind power modeling and control, active distribution networks, and the operation of integrated energy systems.